

## Diffraction Techniques for Nonlamellar Phases of Phospholipids

Lai Ding,<sup>†</sup> Wenhan Liu,<sup>†</sup> Wangchen Wang,<sup>†</sup> Charles J. Glinka,<sup>‡</sup>  
David L. Worcester,<sup>§</sup> Lin Yang,<sup>||</sup> and Huey W. Huang<sup>\*,†</sup>

Department of Physics & Astronomy, Rice University, Houston, Texas 77251,  
Center for Neutron Research, National Institute of Standards and Technology,  
Gaithersburg, Maryland 20899, Biology Division, University of Missouri,  
Columbia, Missouri 65211, and National Synchrotron Light Source,  
Brookhaven National Laboratory, Upton, New York 11973

Received May 24, 2004. In Final Form: July 23, 2004

A neutron diffraction method applicable to nonlamellar phases of substrate-supported lipid membranes is described and validated. When prepared on a flat substrate, the resulting nonlamellar phases have layered symmetry which provides some advantages over powder diffraction for detailed structure determination. This approach recently led to the detection of a rhombohedral phase and a distorted hexagonal phase of lipids. Here the determination of intensity and phase information for such phases is demonstrated by application to the hexagonal phase of diphytanoyl phosphatidylcholine (DPhPC). The hexagonal symmetry is used to verify the data reduction procedure for the intensities of the diffraction peaks. Diffraction intensities measured while varying the D<sub>2</sub>O/H<sub>2</sub>O ratio in the relative humidity was used to solve the phase problem. The neutron scattering length density distribution of the hexagonal phase was constructed and analyzed to elucidate the packing of the lipid molecules. The structure of DPhPC in the hexagonal phase is of interest in connection with its stalk structure in the rhombohedral phase. We also found that the incorporation of tetradecane into the DPhPC hexagonal phase is limited, similar to the case for dioleoyl phosphatidylethanolamine.

Two new lipid structures were discovered recently: a rhombohedral phase that contained the structure of a membrane fusion intermediate state<sup>1,2</sup> and a distorted hexagonal phase in which the binary lipid mixture was speculated to have demixed under stress.<sup>3</sup> Both structures were studied by diffraction from a substrate-supported preparation. In this paper we use the same method to study the hexagonal phase of diphytanoyl phosphatidylcholine (DPhPC). We use this system to discuss a problem of data reduction in this diffraction method and describe its extension to neutron diffraction where a phase determination method is available. Because X-ray and neutron diffraction are the most commonly used methods for studying lipid structures, an improvement of the methods may significantly benefit membrane research.

In the past, powder diffraction was the primary method used for studying lipid structures (except for the lamellar phases), notably by Luzzati's group,<sup>4</sup> who pioneered the lipid structure research and discovered almost all lipid structures in the 1960s, and by Gruner's group<sup>5,6</sup> who

studied the inverted hexagonal phase and revealed the biological importance of nonlamellar promoting lipids. In a substrate-supported thin film, the layers of periodic structures are parallel to the substrate so that one reciprocal vector is normal to the substrate surface. The other reciprocal vectors of the domains are randomly oriented in the plane of the substrate. To obtain the complete diffraction pattern from such a sample, a combination of a scan normal to the plane of the substrate and off-specular reflection is necessary. The relative normalization between these two recordings is not trivial. It needs to be tested and verified. We performed neutron diffraction by this method on the hexagonal phase of DPhPC for two purposes: (1) We make use of the hexagonal symmetry to test and verify the data reduction procedure. (2) To address the question of the phases for the diffraction peaks,<sup>6</sup> we demonstrate a phase-determining method by H<sub>2</sub>O/D<sub>2</sub>O exchange that is applicable to structures for which one can select unit cells with a water center. As a result we solved the structure of the DPhPC hexagonal phase for the first time.

DPhPC is an archaeal phospholipid.<sup>7,8</sup> It forms stable bilayers<sup>9</sup> that exhibit low permeability,<sup>10</sup> so the lipid has been commonly used for making model membranes<sup>11,12</sup> and more recently for biotechnological applications.<sup>13</sup>

\* Address reprint request to Dr. Huey W. Huang. Tel.: 713 3484899. Fax: 713 3484150. E-mail: hw Huang@rice.edu.

<sup>†</sup> Rice University.

<sup>‡</sup> National Institute of Standards and Technology.

<sup>§</sup> University of Missouri.

<sup>||</sup> Brookhaven National Laboratory.

(1) Yang, L.; Huang, H. W. Observation of a membrane fusion intermediate structure. *Science* **2002**, *297*, 1877–1879.

(2) Yang, L.; Huang, H. W. A rhombohedral phase of lipid containing a membrane fusion intermediate structure. *Biophys. J.* **2003**, *84*, 1808–1817.

(3) Yang, L.; Ding, L.; Huang, H. W. New phases of phospholipids and implications to the membrane fusion problem. *Biochemistry* **2003**, *42*, 6631–6635.

(4) Tardieu, A.; Luzzati, V.; Reman, F. C. Structure and polymorphism of the hydrocarbon chains of lipids: a study of lecithin-water phases. *J. Mol. Biol.* **1973**, *75*, 711.

(5) Gruner, S. M. Stability of lyotropic phases with curved interfaces. *J. Phys. Chem.* **1989**, *93*, 7562–7570.

(6) Turner, D. C.; Gruner, S. M. X-ray diffraction reconstruction of the inverted hexagonal (H<sub>II</sub>) phase in lipid-water systems. *Biochemistry* **1992**, *31*, 1340–1355.

(7) Baba, T.; Toshima, Y.; Minamikawa, H.; Hato, M.; Suzuki, K.; Kamo, N. Formation and characterization of planar lipid bilayer membranes from synthetic phytanyl-chained glycolipids. *Biochim. Biophys. Acta* **1999**, *1421*, 91–102.

(8) Baba, T.; Minamikawa, T. H.; Hato, M.; Handa, T. Hydration and Molecular Motions in Synthetic Phytanyl-Chained Glycolipid Vesicle Membranes. *Biophys. J.* **2001**, *81*, 3377–3386.

(9) Hung, W. C.; Chen, F. Y.; Huang, H. W. Order–disorder transition in bilayers of diphytanoyl phosphatidylcholine. *Biochim. Biophys. Acta* **2000**, *1467*, 198–206.

DPhPC exhibited lamellar ( $L_{\alpha}$ ), rhombohedral (R), and hexagonal ( $H_{II}$ ) phases in the temperature range of 20–40 °C. This is similar to dioleoyl phosphatidylcholine and dioleoyl phosphatidylethanolamine (DOPE) mixtures<sup>3</sup>, but DPhPC is the only known pure lipid that exhibits these three phases near physiological temperatures. Therefore, DPhPC is important for the study of the membrane fusion problem, not only for its R phase which contains the structure of the first intermediate state of fusion, stalk,<sup>1,2</sup> but also for its structurally related  $H_{II}$  phase.<sup>14</sup> Both the R and  $H_{II}$  phases of DPhPC have been found so far only in dehydrated conditions.<sup>2</sup> We conjecture that the initial step of membrane fusion is necessarily the removal of water molecules between two contacting bilayers. Thus, fusion must take place in a locally dehydrated condition. This makes the dehydration-induced R and  $H_{II}$  phases relevant to the fusion problem in physiological conditions. Indeed a recent theoretical investigation (Kozlov, private communication) showed that the hydration (or dehydration) energy is the key to the stalk formation. We believe that a molecular construction of the  $H_{II}$  phase based on diffraction results is useful for theoretical as well as molecular simulation studies of the bending transitions from the lamellar phase to the R and  $H_{II}$  phases.

### Experimental Materials and Methods

**Materials.** Diphytanoyl (3,7,11,15-tetramethylhexadecanoic) phosphatidylcholine-d13 (DPhPC) with a deuterated headgroup was purchased from Avanti Polar Lipids (Alabaster, AL). Tetradecane was purchased from Sigma-Aldrich (St. Louis, MO). Perdeuterated tetradecane-d30 was purchased from Cambridge Isotope Laboratories, Inc. (Andover, MA). The 300- $\mu$ m-thick silicon wafers (<100> surface, P-doped) were purchased from Virginia Semiconductor (Fredericksburg, VA). All materials were used as delivered.

**Sample Preparation.** Aligned multilayer samples were prepared by direct deposition of lipid (DPhPC) from an organic solution onto a clean, flat substrate, in this case a silicon wafer. The organic solvent was a 3:1 trifluoroethanol (TFE)–chloroform mixture.<sup>15</sup> A total of 5 mg of lipid was spread over a 25 × 25 mm<sup>2</sup> wafer. The organic solvent was removed in a vacuum or evaporated in open air. The deposit was then hydrated with saturated water vapor at room temperature. Under this condition, the lipid spontaneously formed a stack of hydrated bilayers (in the  $L_{\alpha}$  phase) parallel to the substrate.<sup>15,16</sup> The alignment can be inspected by an X-ray two-dimensional  $\omega$ – $\theta$  scan.<sup>17</sup> DPhPC plus 20 mol % (~6 wt %) tetradecane were codissolved in the organic solvent and prepared the same way.

A U-shaped stand made of copper was used to support the wafers. The seat was 5-mm deep filled with spacers (made of

copper), so the wafers could be inserted vertically. Six wafers inserted into the stand were parallel and separated. The lipid sample on each wafer was in direct contact with ambient air. Such neutron samples were first used by Yang et al.,<sup>18</sup> so the temperature and hydration of the sample could be changed rapidly (within minutes). It was with such samples we first observed crystallization of membrane pores in multilayers.<sup>18</sup>

The sample was pre-examined by X-ray diffraction (described in detail in Yang and Huang)<sup>2</sup>. At 25 °C, it showed three phases, that is,  $L_{\alpha}$ , R, and  $H_{II}$ , as a function of the relative humidity (RH) of the ambient air. From 100 to ~90% RH, the head-deuterated DPhPC(d13) was in the  $L_{\alpha}$  phase, from ~90 to ~80% RH the R phase, and below ~80% the  $H_{II}$  phase. Compared with hydrogenated DPhPC, the R phase region appeared to have moved up by 10% RH (the R phase of hydrogenated DPhPC is between ~80 and ~70% RH).<sup>2</sup> However, hydration by D<sub>2</sub>O (in place of H<sub>2</sub>O) did not seem to affect the phase diagram. Also, very importantly, we found that addition of 20 mol % tetradecane did not, within a few % RH, alter the phase diagram.

In the  $H_{II}$  phase, the diffraction pattern indicated that the lipid tubes formed periodic arrays of two-dimensional hexagonal symmetry, with the axes of the tubes all parallel to the substrate. The sample formed domains of definitive tube orientation. The domain orientation in the plane of the substrate was random.

**Humidity Chamber.** A new humidity chamber<sup>38</sup> was built for this type of experiment at the small angle neutron scattering (SANS) stations in the National Institute of Standards and Technology (NIST), Center for Neutron Research, Gaithersburg, MD. The design is based on a previous version described in Yang et al.<sup>18</sup> A cylindrical cover made of aluminum enclosed the sample and two symmetrically positioned water wells. The sample holder was seated on an aluminum block that served as the base of the chamber. The temperature of the base block was controlled by a circulating cooler/heater. A Eurotherm model X26 temperature/humidity controller monitored a capacitance humidity sensor (HC-610, Ohmic Instruments, Easton, MD) inside the chamber and a temperature probe (platinum RTD, Omega Engineering) embedded in the copper sample support. The controller outputs a voltage control signal to a bipolar direct current power supply (Kepco model BOP20-10D) that responds by sending current to a pair of thermoelectric cooling/heating elements attached to the water wells. The wells are heated or cooled, depending on the direction of current flow, to raise or lower, respectively, the RH in the chamber to a preset value in the range from 0 to 95% RH with approximately 3% accuracy and 1% repeatability. Structural changes in the sample including phase transitions were observed by neutron diffraction. We could see that the structural changes followed the humidity changes instantaneously.

**Neutron Experiment.** The neutron experiment was performed at the NG7 SANS station in NIST.<sup>19</sup> A rectangular slit of 12 mm (height) × 8 mm (width) was used to define the incident neutron beam. The neutron wavelength was 5 Å with an 11% spread, full width at half-maximum. The area detector (640 × 640 mm<sup>2</sup>, 5 mm resolution) was positioned 875 mm from the sample, and its center was 250 mm transverse to the beam direction. The resulting  $q$  range was 0.03–0.7 Å<sup>-1</sup>. The procedure for sample alignment normally used in X-ray diffraction<sup>20</sup> was not applicable here, because the beam cross section was large and its collimation was not as good as X-rays. However, the attenuation of the scattering by the silicon wafers cast a line shadow on the detector in the direction of the plane of the wafers (see Figure 1). Thus the incident angle  $\omega$  (between the incident beam and the plane of the substrate) can be determined from the position of the shadow relative to the transmitted beam center. The experiment was conducted at temperature 25 °C and 58% RH at five D<sub>2</sub>O/H<sub>2</sub>O ratios: 0:1, 1:3, 1:1, 3:1, and 1:0.

(10) Dannenmuller, O.; Arakawa, K.; Eguchi, T.; Kakinuma, K.; Blanc, S.; Albrecht, A.-M.; Schumtz, M.; Nakatani, Y.; Ourisson, G. Membrane properties of archaeal macrocyclic diether phospholipids. *Chem.–Eur. J.* **2002**, *6*, 645–654.

(11) Redwood, W. R.; Pfeiffer, F. R.; Weisbach, J. A.; Thompson, T. E. Physical properties of bilayer membranes formed from a synthetic saturated phospholipid in *n*-decane. *Biochim. Biophys. Acta* **1971**, *233*, 1–6.

(12) Akeson, M.; Branton, D.; Kasianowicz, J. J.; Brandin, E.; Deamer, D. W. Microsecond time-scale discrimination among polycytidylic acid, polyadenylic acid and polyuridylic acid as homopolymers or as segments within single RNA molecules. *Biophys. J.* **1999**, *77*, 3227–3233.

(13) Gambacorta, A.; Gliozzi, A.; de Rosa, M. Archaeal lipids and their biotechnological applications. *World J. Microbiol. Biotechnol.* **1995**, *11*, 115–131.

(14) Siegel, D. P. The modified stalk mechanism of lamellar/inverted phase transitions and its implications for membrane fusion. *Biophys. J.* **1999**, *76*, 291–313.

(15) Ludtke, S.; He, K.; Huang, H. W. Membrane thinning caused by magainin 2. *Biochemistry* **1995**, *34*, 16764–16769.

(16) He, K.; Ludtke, S. J.; Worcester, D. L.; Huang, H. W. Neutron scattering in the plane of membrane: structure of alamethicin pores. *Biophys. J.* **1996**, *70*, 2659–2666.

(17) Weiss, T. M.; van der Wel, P. C. A.; Killian, J. A.; Koeppe, R. E., II; Huang, H. W. Hydrophobic mismatch between helices and lipid bilayers. *Biophys. J.* **2003**, *84*, 379–385.

(18) Yang, L.; Weiss, T. M.; Lehrer, R. I.; Huang, H. W. Crystallization of antimicrobial pores in membranes: magainin and protegrin. *Biophys. J.* **2000**, *79*, 2002–2009.

(19) Glinka, C. J.; Barker, J. G.; Hammouda, B.; Krueger, S.; Moyer, J. J.; Orts, W. J. The 30 m Small-Angle Neutron Scattering Instruments at the National Institute of Standards and Technology. *J. Appl. Crystallogr.* **1998**, *31*, 430–445.

(20) Wu, Y.; He, K.; Ludtke, S. J.; Huang, H. W. X-ray diffraction study of lipid bilayer membrane interacting with amphiphilic helical peptides: diphytanoyl phosphatidylcholine with alamethicin at low concentrations. *Biophys. J.* **1995**, *68*, 2361–2369.

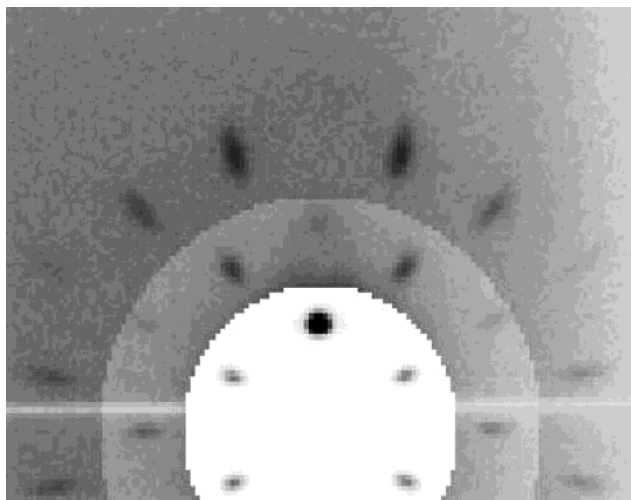


**Figure 1.** Detector image of off-specular reflection from pure DPhPC(d13) at 25 °C and 58% RH of pure H<sub>2</sub>O. To show all the peaks, the intensities of three regions are on different scales: the second shell is 100 times that of the central region, and the outer region is 160 times. The  $q_z$  axis is vertical through the strongest peak (0, 1). The horizontal axis is approximately proportional to the  $q_x$  axis, so the image corresponds approximately to the reciprocal lattice shown in Figure 2. The horizontal white line is the shadow of the silicon wafers that was utilized to define the incident angle  $\omega$ .

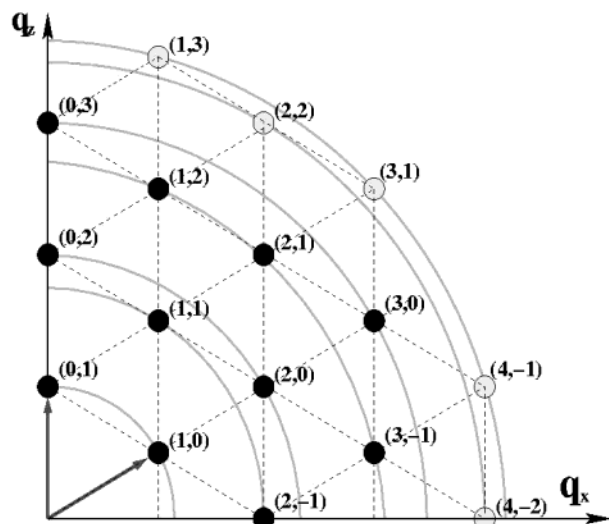


**Figure 2.** Reciprocal lattice of the hexagonal phase. The black dots are the detected peaks. The reciprocal lattice constant is  $0.14 \text{ \AA}^{-1}$ .

**Off-Specular Reflection.** As described in Introduction, the in-plane orientations of the crystal domains are powdered (randomly distributed). Consequently, in the reciprocal space, the lattice points are distributed in a series of rings parallel to the substrate and centered around an axis  $q_z$  normal to the plane. The in-plane reciprocal vector will be called  $\mathbf{q}_r$ . Each point on the two-dimensional detector corresponds to a  $(q_z, \mathbf{q}_r)$ . Each ring of lattice points will be registered as a diffraction peak on the detector if the ring intercepts the Ewald sphere. For a hexagonal phase of lipid, the reciprocal lattice is two-dimensional. One axis is  $q_z$  and the in-plane axis will be called  $q_x$  (instead of  $\mathbf{q}_r$ ). The reciprocal lattice of the hexagonal phase is shown in Figure 2.

At  $\omega = 1.6^\circ$  the area detector covered all detectable Bragg peaks of the hexagonal phase (Figure 1), except for those along  $q_z$ . The reason that the first two peaks on  $q_z$  (0, 1) and (0, 2), appeared in the reflection was the combination of (1) the inevitable mosaic of the sample that was discussed in Yang et al.<sup>21</sup> and (2) the angular divergence of the neutron beam. The (0, 1) peak is particularly strong because it is close to satisfying the Bragg

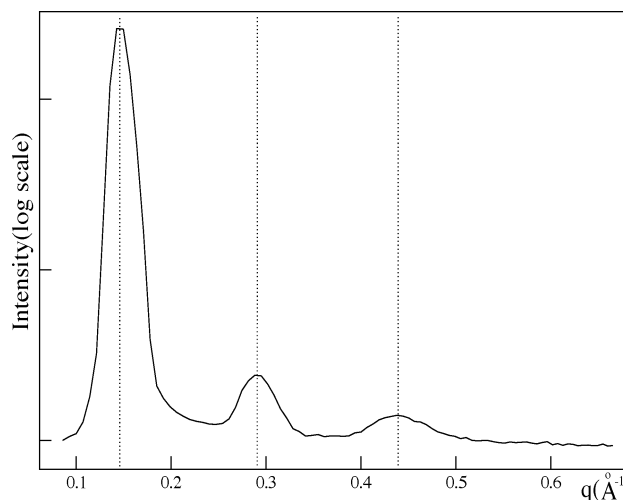


**Figure 3.** Composite data of the oscillating- $\omega$  scan for pure DPhPC(d13) at 25 °C and 58% RH of pure H<sub>2</sub>O.

condition. All peaks on  $q_z$  will be integrated correctly by the oscillating- $\omega$  scan described below. Off the  $q_z$  axis, there were eight independent peaks detected as shown in Figure 2, designated by the hexagonal indices ( $H$ ,  $K$ ). The data were collected for 3 h for each sample and for each of five D<sub>2</sub>O/H<sub>2</sub>O ratios.

**Oscillating- $\omega$  Scan.** The peaks along  $q_z$  were scanned by rotating the angle  $\omega$ . (Here we follow the convention of calling  $2\theta$  the angle between the incident beam and the diffraction beam and  $\omega$  is the angle between the incident and the plane of substrate.) Data were collected as  $\omega$  was increased in steps  $\Delta\omega = 0.25^\circ$ , 3 min per step, from  $\omega = 0$  to  $\omega \sim 13^\circ$ . The complete data of oscillating- $\omega$  scan was the sum of a series of files, each collected at one  $\omega$ -step.

**Data Reduction.** The data on the two-dimensional detector were first treated by the standard correction procedure<sup>22</sup> for the instrumental background and detector sensitivity.

(1) *Off-Specular Reflection.* The intensities of the diffraction peaks were integrated directly on the detector image in the following manner. The peaks were first integrated in the  $q_x$  direction over a width slightly wider than the apparent peak widths. The result was plotted along the  $q_z$  axis. On this one-dimensional profile, the background was obtained by using the intensities between the peaks and extrapolated into the peak regions. After the background removal, each peak was integrated along the  $q_z$  direction.

(2) *Oscillating- $\omega$  Scan.* All the data at different  $\omega$  were summed to obtain one diffraction pattern along  $q_z$  (Figure 3). The peak intensities were integrated in the same manner as for the off-specular reflection.

The integrated peak intensities  $E$  were then reduced to obtain the magnitudes of the relative amplitudes  $F$  for the unit-cell form factor. The procedure of the reduction was described in Yang and Huang<sup>2</sup> and is recapitulated in Table 1. In comparison with the formulas given in ref 2, note the typos in the latter including the definitions for angles  $\nu$  and  $\gamma$  and expressions for  $C_{\text{abs}}$ . Also in Table 1 we have eliminated the redundant angles  $\beta$  and  $\omega$  used in ref 2.

## Results and Discussion

**Normalization between the Off-Specular Scan and the Oscillating- $\omega$  Scan.** It is a standard practice that one obtains integrated peak intensities from a single

(21) Yang, L.; Weiss, T. M.; Harroun, T. A.; Heller, W. T.; Huang, H. W. Supramolecular structures of peptide assemblies in membranes by neutron off-plane scattering: Method of analysis. *Biophys. J.* **1999**, *77*, 2648–2656.

(22) SANS Data Reduction with IGOR Pro. [http://www.ncnr.nist.gov/programs/sans/manuals/data\\_red.html](http://www.ncnr.nist.gov/programs/sans/manuals/data_red.html) (accessed 2004).

**Table 1. Formula for Data Reduction,  $E = I_0 F^2 C_p C_L C_{abs} C_{geo} \Delta T^2$** 

| off-specular reflection   | $\omega$ scan   |
|---|---|
| $C_p^b = \sin^2 \psi$   | $C_p^b = \cos^2 2\theta$  |
| $C_L = 1/\cos \alpha \cos \nu \sin \gamma$  | $C_L = 1/\sin 2\theta$  |
| $C_{abs} = \frac{1 - \exp\left[-\mu a \left(\frac{1}{\sin \nu} + \frac{1}{\sin \alpha}\right)\right]}{\mu a \left(\frac{1}{\sin \nu} + \frac{1}{\sin \alpha}\right)}$ | $C_{abs} = \frac{[1 - \exp(-2\mu a/\sin\theta)]\sin\theta}{2\mu a}$ |
| $C_{geo} = \frac{b/\sin \alpha}{w}$<br>or 1 if greater than 1   | $C_{geo} = \frac{b/\sin \alpha}{w}$<br>or 1 if greater than 1       |
| $\Delta T$  | $2\pi/\Omega$   |

<sup>a</sup> Notations:  $\psi$  = the angle between the incident polarization vector and the scattered beam;  $\alpha$  = the angle between the incident beam and the substrate surface (the  $x$ - $y$  plane);  $\nu$  = the angle between the diffracted beam and the  $x$ - $y$  plane;  $\gamma$  = the angle between the in-plane ( $x$ - $y$ ) projection of the incident beam and the in-plane projection of the diffracted beam;  $\mu$  = the linear absorption coefficient of the sample;  $\mu_s$  = the linear absorption coefficient of substrate;  $a$  = the sample thickness;  $a_s$  = the substrate thickness;  $C_{geo}$  is the ratio of the length of the beam footprint  $b/\sin \alpha$  over the length of the sample;  $\Delta T$  is the scan time; and  $\Omega$  is the angular velocity of the  $\omega$  scan. <sup>b</sup> The polarization factor  $C_p$  is for X-ray diffraction only. <sup>c</sup>  $C_{abs}$  in the table is for reflection geometry. For transmission geometry the absorption correction is

$$C_{abs} = \exp\left[\frac{-\mu_s a_s + \mu a}{\sin \alpha}\right] \frac{1 - \exp\left[-\mu a \left(\frac{1}{\sin \nu} - \frac{1}{\sin \alpha}\right)\right]}{\mu a \left(\frac{1}{\sin \nu} - \frac{1}{\sin \alpha}\right)}$$

crystal by collecting the diffraction intensity while rotating the sample,<sup>23</sup> as in the oscillating- $\omega$  scan. On the other hand one obtains integrated peak intensities directly from powder diffraction because the sample can be regarded as rotating without change. Here we have an unusual situation that one part of the diffraction pattern was obtained from an oscillating- $\omega$  scan and another part of the pattern was from an off-specular reflection that was an in-plane powder diffraction. We are not aware of similar examples in the literature. Therefore, it is essential to verify the relative normalization between the two scans as set forth by Yang and Huang.<sup>2</sup>

The relative normalization is given in the last row of Table 1;  $\Delta T$  for the off-specular reflection and  $2\pi/\Omega$  for the oscillating- $\omega$  scan. Using the standard scanning program of NIST, the data files were all normalized to a fixed number of incident neutrons, including the data file for the 3-h off-specular reflection and each 3-min data file at each  $\omega$  step in the oscillating- $\omega$  scan, as if each data file was recorded over the same period of time. Thus, we take  $\Delta T$  as 1. Then the angular velocity  $\Omega$  (Table 1) is the step size for the oscillating- $\omega$  scan expressed in radians divided by  $\Delta T$ ,  $\pi(0.25/180)/\Delta T$ , so  $2\pi/\Omega = 1440$ .

In Figure 2, we see that the peaks on the same circle are related by the hexagonal symmetry, and they should have the same magnitude. This symmetry requirement can be used to test our data reduction procedure between the peaks measured by the off-specular reflection and those measured by the oscillating- $\omega$  scan. The results are shown in five panels of Figure 4. Each panel contains a set of symmetrically related peaks. The errors of the experimental values in Figure 4 are difficult to assess precisely. The largest source of error was from the uncertainties in the background removal. We estimated this error for every peak individually. In comparison, the statistical errors

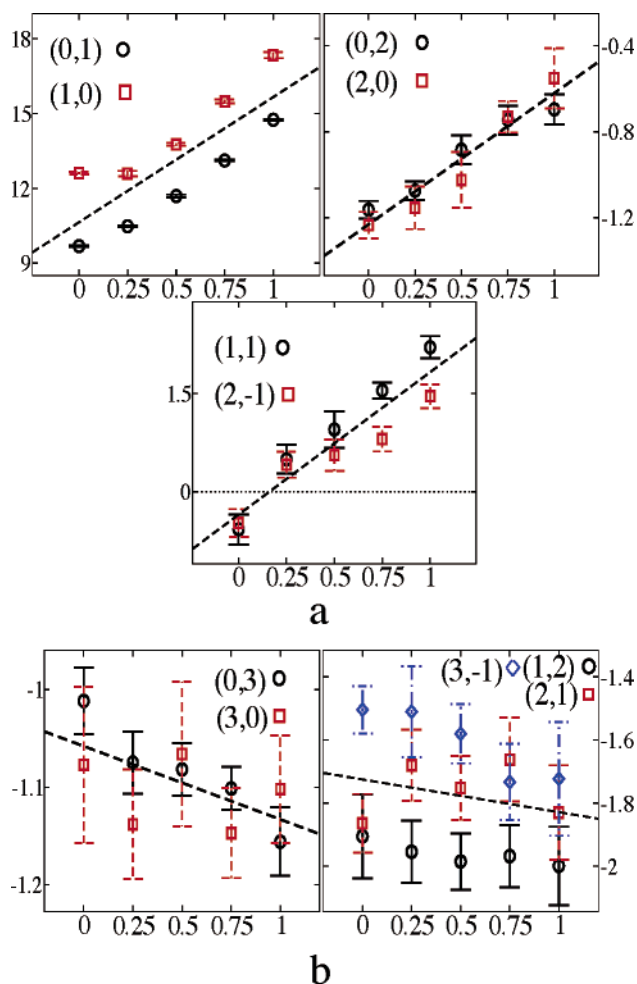


**Figure 4.** Diffraction amplitudes (in an arbitrary unit) of pure DPhPC(d13) plotted as a function of  $x$ , the  $D_2O/H_2O$  fraction in the  $D_2O/H_2O$  mixture used to hydrate the lipid. The error bars for (0, 1) and (1, 0) are within the symbols. The straight line in each panel was a fit to the average amplitudes for each peak and its symmetric equivalents. (a) The phases for the peaks on the first three rings of Figure 2 can be determined with confidence by requiring a positive slope. (b) The phases for the peaks on the fourth and fifth rings of Figure 2 are determined by requiring that the resulting density map is physically reasonable (see Figure 5 and text).

from the neutron counts are insignificant. The possible error on the  $D_2O/H_2O$  content in the sample, that is, the error bar on the horizontal axis of Figure 4, is unknown. Considering the large factor involved in the relative normalization, the integrated intensities of symmetrically related peaks agree with each other quite well. We take this as a proof for the correctness of our reduction procedure.

**Phase Determination by  $D_2O/H_2O$  Exchange.** We now show that the diffraction phases of the hexagonal structure can be determined by  $D_2O/H_2O$  exchange. The diffraction amplitude from a lipid-water system is given by<sup>24</sup>

$$A_H(\mathbf{q}) = \sum_{i \in L} b_i e^{i\mathbf{q} \cdot \mathbf{r}_i} + \sum_{j \in W} b_j^{H_2O} e^{i\mathbf{q} \cdot \mathbf{r}_j} \quad (1)$$

where  $b_i$  stands for the coherent scattering amplitude or the scattering length of the  $i$ th element at position  $\mathbf{r}_i$ . We have separated the sum over the elements to two parts,

(23) Warren, B. E. *X-ray Diffraction*; Dover: New York, 1969; pp 41–49.

(24) Bacon, G. E. *Neutron Diffraction*; Clarendon Press: Oxford, 1975; pp 21–50.

for lipid (L) and for water (W). If part of water is replaced by D<sub>2</sub>O, the amplitude can be written as

$$A_{\text{DH}}(\mathbf{q}) = \sum_{i \in L} b_i e^{i\mathbf{q} \cdot \mathbf{r}_i} + \sum_{j \in W} [b_j^{\text{H}_2\text{O}} + x(b_j^{\text{D}_2\text{O}} - b_j^{\text{H}_2\text{O}})] e^{i\mathbf{q} \cdot \mathbf{r}_j} = A_{\text{H}}(\mathbf{q}) + xRA_{\text{D}_2\text{O}}(\mathbf{q}) \quad (2)$$

where  $x$  is the D<sub>2</sub>O fraction of the D<sub>2</sub>O/H<sub>2</sub>O mixture,  $R = \{(b_j^{\text{D}_2\text{O}} - b_j^{\text{H}_2\text{O}})\}/\{b_j^{\text{D}_2\text{O}}\}$  is a positive constant, and  $A_{\text{D}_2\text{O}}(\mathbf{q})$  is the diffraction amplitude if only the water (D<sub>2</sub>O) molecules in the lipid–water system contribute to the diffraction. Equation 2 has two applications.

(1) Experiment determines only the absolute magnitude of the amplitude. If a diffracting system is centrosymmetric, its diffraction amplitudes are real. In that case, the magnitude  $|A_{\text{DH}}(\mathbf{q})|$  varies linearly with  $x$ . On the other hand, if the diffraction amplitudes are complex, the magnitude  $|A_{\text{DH}}(\mathbf{q})|$  is in general not a linear function of  $x$ . Therefore, a plot of the magnitude  $|A_{\text{DH}}(\mathbf{q})|$  as a function of  $x$  provides a test for whether the system is centrosymmetric or not. This method was first used by Bragg and Perutz.<sup>25</sup>

(2) If the system is centrosymmetric,  $A_{\text{DH}}(\mathbf{q})$ ,  $A_{\text{H}}(\mathbf{q})$ , and  $A_{\text{D}_2\text{O}}(\mathbf{q})$  are all real and either positive or negative. Then there are three possible cases for the experimental values of  $|A_{\text{DH}}(\mathbf{q})|$ : it either linearly increases or decreases with  $x$  or it linearly decreases with  $x$  to 0 and then linearly increases. Because  $A_{\text{D}_2\text{O}}(\mathbf{q})$  determines the slope of  $A_{\text{DH}}(\mathbf{q})$  as a function of  $x$ , in each case if the sign of  $A_{\text{D}_2\text{O}}(\mathbf{q})$  is known, the sign of  $A_{\text{DH}}(\mathbf{q})$  is determined. In general it is much easier to model the water distribution alone than to model the whole lipid–water system. That is why this method of phase determination is useful.

The simplest case is when it is possible to select a unit cell so that water is confined near the center, such as the H<sub>II</sub> phase. Let the unit cell be a hexagon enclosing the cross section of one H<sub>II</sub> tube, that is, the Wigner–Seitz cell. Then the water molecules can be reasonably assumed to be in a Gaussian distribution centered at the origin of the unit cell. Hence, all water amplitudes  $A_{\text{D}_2\text{O}}(\mathbf{q})$  are positive. This implies that the signs of  $A_{\text{DH}}(\mathbf{q})$  and  $A_{\text{H}}(\mathbf{q})$  must be chosen so that  $A_{\text{DH}}(\mathbf{q})$  has a positive slope as a function of  $x$ . Using this method, the phases of the peaks on the first three rings (Figure 2) can be determined with confidence as shown in Figure 4a. The peaks on the fourth and the fifth rings (Figure 2) are problematic for two reasons. (1) The slopes are small, and their signs cannot be determined within the experimental errors (Figure 4b). A small slope implies a small water amplitude  $A_{\text{D}_2\text{O}}(\mathbf{q})$ . (2) The sign of a small water amplitude at large  $q$  ( $> \pi/r_0$ ,  $r_0$  being the radius of the water column) is sensitive to the deviation of the water distribution from a presumed Gaussian form. For these two reasons, we could not determine with confidence the signs of  $A_{\text{DH}}(\mathbf{q})$  on the fourth and the fifth rings by the  $x$  dependence.

Therefore, we examined the consequences of all possible phase assignments. With each set of phase assignments, the diffraction amplitudes were used to construct the unnormalized neutron scattering density in the unit cell:

$$\rho(\mathbf{r}) = \sum_{H,K} A_{\text{DH}}(\mathbf{q}_{H,K}) \cos(\mathbf{q}_{H,K} \cdot \mathbf{r}) \quad (3)$$

The results of DPhPC(d13) with pure H<sub>2</sub>O hydration are shown in Figure 5. The assignment (+, −) and (−, +) for the peaks on the fourth and fifth rings, respectively, can

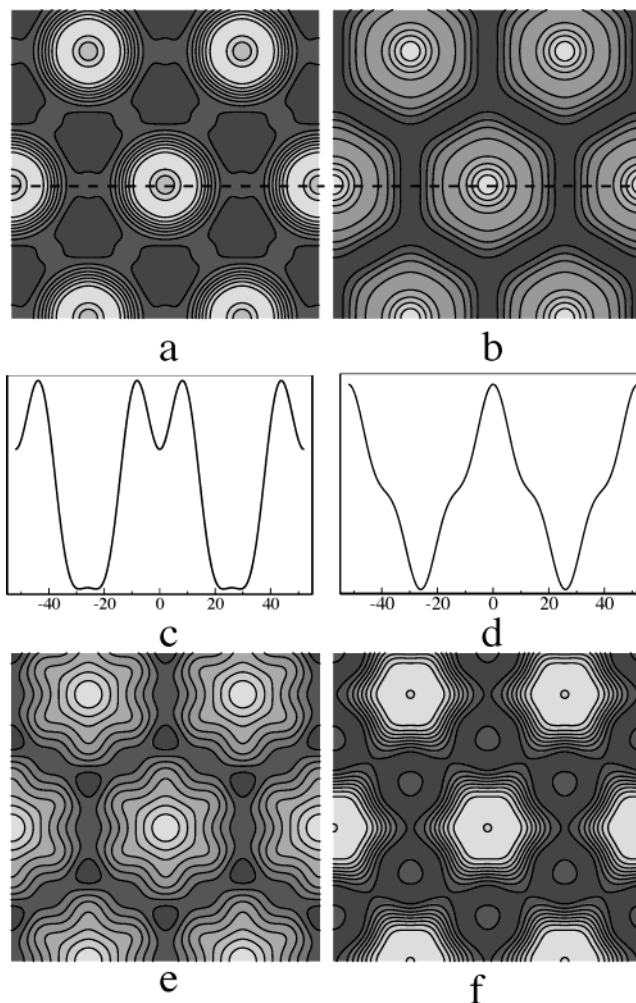


**Figure 5.** Neutron scattering length density map of pure DPhPC(d13) in the hexagonal phase hydrated by H<sub>2</sub>O for four different phase assignments for the diffraction peaks on the fourth and fifth rings of Figure 2. (a) Phase assignment (−, −) for the peaks on the fourth and fifth rings, respectively. (b) (+, +). (c) (+, −). (d) (−, +). (e) (+, −). (f) (−, +). (c) The density profile along the dashed line shown in part a. (d) The density profile along the dashed line shown in part b.

**Table 2.** Calculated Neutron Scattering Length Density (10<sup>9</sup> cm<sup>−2</sup>)

|  | Calculated Neutron Scattering Length Density (10 <sup>9</sup> cm <sup>−2</sup> ) |
|--|--|
| headgroup [phosphorylcholine(d13) + glycerol + carbonyl] | 68   |
| chain of DPhPC minus 2CH <sub>3</sub>                    | −1.9   |
| CH   | 14   |
| CH <sub>2</sub>  | −2.9   |
| CH <sub>3</sub>  | −8.3   |
| tetradecane  | −4.3   |
| tetradecane(d30)   | 68   |
| H <sub>2</sub> O   | −5.4   |
| D <sub>2</sub> O   | 65   |

be excluded immediately. (+, −) gave a physically unreasonable star shape to the H<sub>II</sub> tube (Figure 5c). The density of (−, +) is also star-shaped and furthermore has a local maximum of scattering length density at the corners of the unit cell where the density should be the lowest (Figure 5d). Each chain of DPhPC has two terminal methyl groups that have the lowest density (Table 2). The density maps corresponding to the assignments (−, −) and (+, +) are shown in Figure 5a,b. The density profiles along a line through the centers of unit cells are also shown (Figure 5, middle row). The profile of (−, −) has an expected dip at the water center whereas (+, +) has the maximum

(25) Bragg, W. L.; Perutz, M. F. The external form of the hemoglobin molecule. I. *Acta Crystallogr.* **1952**, *5*, 277–283.

density at the water center. Thus, we concluded that the most reasonable phase assignment is negative for all peaks on the fourth and fifth rings. These phases are shown in Figure 4b. The phases for DPhPC + 20 mol % tetradecane were determined the same way. The addition of tetradecane did not alter the phases.

This method of phasing by D<sub>2</sub>O/H<sub>2</sub>O exchange was previously applied to bilayer lipid structures<sup>26</sup> as an extension of procedures and examples in neutron crystallography.<sup>27</sup> Subsequently there were several applications to phasing the diffraction amplitudes from bilayer structures.<sup>26,28–30</sup> However, higher hydrations in bilayers often result in widths and shapes of the water distributions that limit the use of this phasing procedure (see, for example, the highest hydration data in Worcester and Franks).<sup>28</sup>

This method is also analogous to the method of multiwavelength anomalous diffraction, where diffraction measurements are carried out at several X-ray energies above and below the absorption edge of anomalous scatterers (e.g., Se, which often replaces the S in a disulfide bond). The diffraction amplitude of each peak is now a superposition of the normal scattering, which is constant of X-ray energy, and the anomalous scattering, which is proportional to the atomic scattering factor of the anomalous scatterer that changes with X-ray energy. The energy dependence of the anomalous scattering factor is known, so this factor plays the role of  $x$  of eq 2. Because there are usually only a handful (<10) of anomalous scatterers in one unit cell, the distribution of them can be determined by the direct method, solely from the anomalous amplitudes. Knowing the phase angles of the anomalous amplitudes solves the phases of the normal amplitudes.

**Hexagonal Structure of DPhPC and the Effect of Tetradecane.** The scattering length density map of DPhPC(d13) with H<sub>2</sub>O hydration (Figure 5a) and the corresponding map with D<sub>2</sub>O hydration (not shown) are used to analyze the lipid molecular distribution in the unit cell. The unnormalized neutron scattering length density  $\rho$  calculated by eq 3 is related to the true density  $\rho_0$  by two constants:  $\rho_0 = a\rho + b$ , where  $b$  is due to the absence of the zeroth order amplitude. However, the lack of normalization does not affect the shape of the constant density contours. One surprising result is that the H<sub>II</sub> tube of DPhPC seems to be quite circular, particularly in comparison with that of DOPE.<sup>31</sup>

To get an idea of how the lipid packs the H<sub>II</sub> tube, we will first try to find the regions for water, for the lipid headgroups, and for the chains. It is well-known water penetrates the headgroup region, but its amount is unknown a priori. This problem can be solved by H<sub>2</sub>O/D<sub>2</sub>O exchange. The lattice constant is 52 Å between two closest hexagonal centers or 26 Å from the center to each side of the hexagonal unit cell. Table 2 lists the calculated

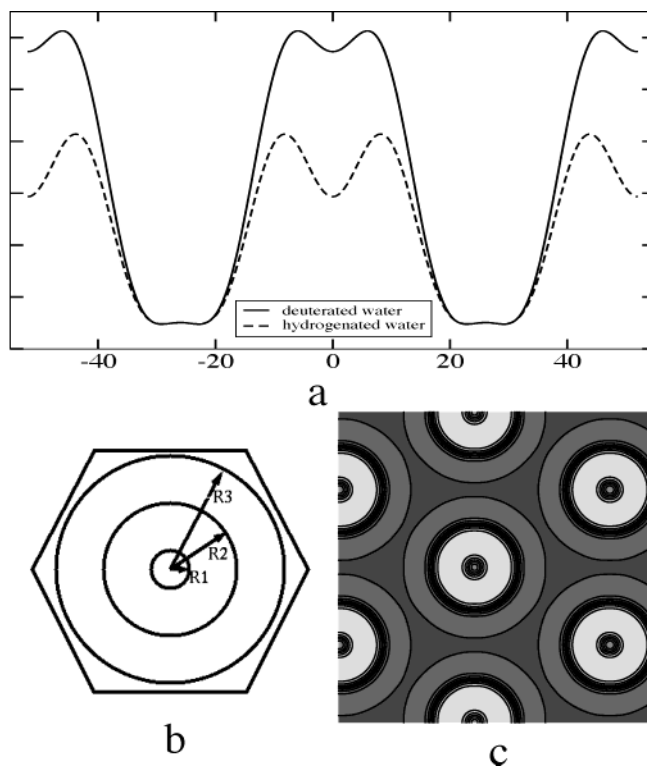


**Figure 6.** (a) Comparison of two density profiles as Figure 5c, one for D<sub>2</sub>O hydration (solid line) and one for H<sub>2</sub>O hydration (dashed line). (b) The model with variable radii that was used to analyze the lipid packing. (c) The model that most closely fit the data.

neutron scattering length densities for different parts of the DPhPC molecule, where the phospholipid component volumes are taken from Armen et al.<sup>32</sup> Because of the nearly circular density contours, we divide a unit cell into several circular shells as shown in Figure 6b: from the center to radius  $R_1$  is the water density  $-5.4$  (in the units of  $10^9 \text{ cm}^{-2}$ ; see Table 2), from radius  $R_1$  to  $R_2$  is the headgroup/water region filled with density 45 (see next paragraph), from  $R_2$  to  $R_3$  is  $-1.9$ , the density of the chains excluding 2 terminal  $\text{CH}_3$ , and from  $R_3$  to the boundary of the unit cell is  $-8.3$ , the density of  $\text{CH}_3$ .

In Figure 6a, we show the comparison of two density profiles through the same line shown in Figure 5a, one for the density map of H<sub>2</sub>O hydration (dotted line) and one for the density map of D<sub>2</sub>O hydration (solid line). Because these two profiles were obtained from the same sample under the same condition except for exchanging H<sub>2</sub>O with D<sub>2</sub>O, the normalization constant  $a$  is the same for both. We relatively normalized them (making them equal) in the chain tail region where water should make no contribution to the density, which would make the normalization constant  $b$  the same for both. Because the scattering length density of D<sub>2</sub>O (65) is practically the same as that of the deuterated headgroup (68), we let the headgroup density of D<sub>2</sub>O hydration be 68. Then the headgroup density relative to the chain region should be  $68 + 1.9$  (Table 2) for D<sub>2</sub>O hydration. The density ratio of the headgroup (relative to the chains) between the D<sub>2</sub>O hydration and the H<sub>2</sub>O hydration on Figure 6a is  $68 + 1.9$  to  $45 + 1.9$ . That is why we used 45 for the density of the headgroup region for H<sub>2</sub>O hydration.

(26) Worcester, D. L. Neutron Beam Studies of Biological Membranes and Membrane Components. In *Biological Membranes*; Chapman, D., Wallach, D. F. H., Eds; Academic Press: London, 1976; Vol. 3.

(27) Speakman, J. C. In *Chemical Applications of Thermal Neutron Scattering*; Willis, B. T. M., Ed.; Oxford University Press: New York, 1973; pp 214–215.

(28) Worcester, D. L.; Franks, N. P. Structural Analysis of Hydrated Egg Lecithin and Cholesterol Bilayers II. Neutron Diffraction. *J. Mol. Biol.* **1973**, *100*, 359–378.

(29) Franks, N. P.; Arunachalam, T.; Caspi, E. Direct method for determination of membrane electron-density profiles on an absolute scale. *Nature* **1978**, *276*, 530–532.

(30) Franks, N. F.; Lieb, W. R. The structure of lipid bilayers and the effects of general anaesthetics. *J. Mol. Biol.* **1979**, *133*, 469–500.

(31) Turner, D. C.; Gruner, S. M.; Huang, J. S. Distribution of decane within the unit cell of the inverted hexagonal (H<sub>II</sub>) phase of lipid-water-decane systems determined by neutron diffraction. *Biochemistry* **1992**, *31*, 1356–1363.

(32) Armen, R. S.; Uitto, O. D.; Feller, S. E. Phospholipid component volumes: determination and application to bilayer structure calculations. *Biophys. J.* **1998**, *75*, 734–744.

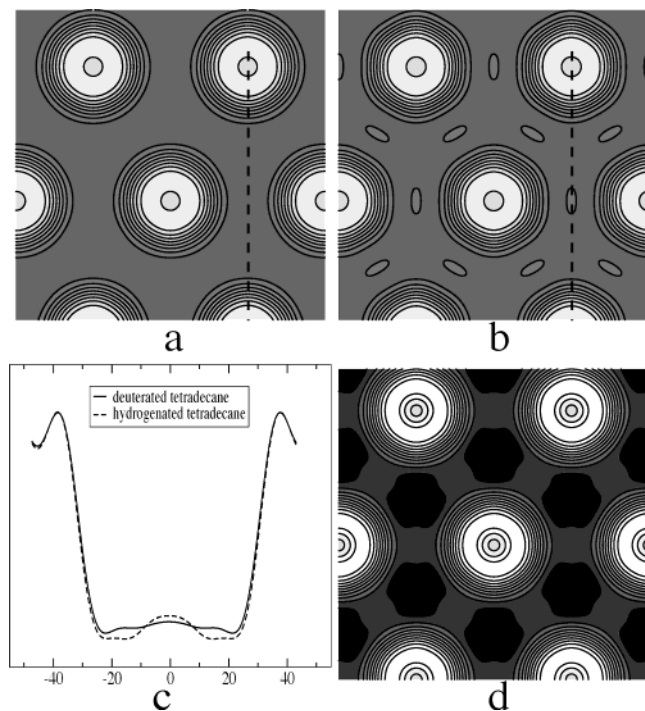


**Figure 7.** (a) Scattering length density of DPhPC(d13) + hydrogenated tetradecane hydrated with H<sub>2</sub>O. (b) The scattering length density of DPhPC(d13) + deuterated tetradecane hydrated with H<sub>2</sub>O. (c) The comparison of the density profiles along the dashed line shown in parts a and b. The two profiles are normalized to each other at the headgroup region. (d) For comparison we reproduced the density of DPhPC(d13) without tetradecane (same as Figure 5a).

From the model we calculate the model amplitude  $A_H^{\text{model}}(\mathbf{q})$ . We then sought the minimum of

$$\Delta = \sum_{H,K} |A_H^{\text{model}}(\mathbf{q}_{H,K}) \exp(-u^2 \mathbf{q}_{H,K}^2) - \alpha A_H(\mathbf{q}_{H,K})| \quad (4)$$

by varying  $R_1$ ,  $R_2$ ,  $R_3$ , and  $u^2$  where  $\exp(-u^2 \mathbf{q}_{H,K}^2)$  represents the Debye–Waller factor. The constant  $\alpha$  was chosen so that the term for  $(H, K) = (0, 1)$  in eq 4 vanished. The best result was shown in Figure 6c that has the following values:  $R_1 = 2.9 \text{ \AA}$ ,  $R_2 = 14.6 \text{ \AA}$ ,  $R_3 = 25 \text{ \AA}$ ,  $u = 2 \text{ \AA}$ . We then considered a slice of the H<sub>II</sub> tube of 9 Å in thickness. The 9 Å is the approximate linear dimension of the DPhPC cross section that was estimated to be about 80 Å<sup>2</sup> in a bilayer.<sup>9,20</sup> Within this hexagonal cylinder, we found that the volume exterior to the radius  $R_2$  fits the chains of 12 lipid molecules. The volume within the radius  $R_2$  fits 12 headgroups and 91 water molecules. Thus, at 58% RH every lipid associates with about 7.6 water molecules. This is in general agreement with an NMR measurement<sup>33</sup> where each DPhPC molecule was found to be hydrated by ~5 water molecules in the hexagonal phase (its equivalent RH was unknown). Thus, there are in average 12 DPhPC molecules in a cross section of the H<sub>II</sub> tube.

Next we consider the effect of tetradecane. The constructed density maps of DPhPC(d13) + tetradecane (20 mol %) and DPhPC(d13) + tetradecane(d30) (20 mol %) are shown in parts a and b of Figure 7, respectively. Within the experimental errors, the addition of 20 mol %

tetradecane did not change the lattice constant. This is similar to the case of DOPE where the lattice constant did not change for 5–20 wt % (16–67 mol %) added tetradecane.<sup>34</sup> More surprisingly there is very little difference between the addition of deuterated tetradecane and the addition of hydrogenated tetradecane. This could only mean that very little tetradecane was actually incorporated into the hexagonal phase, at least by our method of preparation. Because the lipid distributions with *d*-tetradecane and with *h*-tetradecane are supposed to be the same, we normalize the headgroup region of the density maps between the two. The profiles along the lines marked in Figure 7a,b are shown in part c. The difference is small and, as we expected, is confined in the region exterior to the radius  $R_3$  in the model. To explain the difference between these two profiles, one with *d*-tetradecane and another with *h*-tetradecane, we can show that there was at most 0.84 tetradecane molecules in the volume of 12 lipid molecules. This means that at most 7 mol % tetradecane was actually incorporated in the hexagonal phase of DPhPC even though 20 mol % of tetradecane was codissolved with DPhPC in the sample preparation.

## Summary

Theoretically one might expect the H<sub>II</sub> tube of pure lipid to be somewhat hexagonal in its cross section because of the confines of the hexagonal unit cell. This idea seemed to have born out in the case of DOPE.<sup>6</sup> DPhPC with its bulky chains is apparently different. Its density distribution appears to be quite circular in the H<sub>II</sub> tube. The structure incorporates a limited amount of tetradecane, at most 7% in molar ratio or 2% in weight ratio, and it has little effect on the size of the DPhPC unit cell. Consistent with these results from the structural analyses, tetradecane also did not affect the L<sub>α</sub>-R-H<sub>II</sub> phase diagram of DPhPC. We believe that these experimental results are useful for the energy computations concerning membrane fusion.<sup>14,35–37</sup>

The diffraction method used here has some apparent advantages over powder diffraction. Figure 2 shows that the circles represent the positions of the powder diffraction rings. It is clear that some neighboring rings will overlap in powder diffraction that will make the measurement of intensity significantly difficult. The neutron powder diffraction of DOPE<sup>31</sup> detected four rings, but the errors for the weak rings were as much as 50–100%. By the present method, we detected one more order and all peaks were well separated; thus, their integrated intensities were much more accurately measured. Perhaps the clearest advantage of the present method is the apparent lattice symmetry shown on the two-dimensional detector. For instance, a distorted hexagonal phase was readily identified by this method as reported in Yang et al.<sup>3</sup>, which would be very difficult to detect by powder diffraction.

(34) Rand, R. P.; Fuller, N. L.; Gruner, S. M.; Parsegian, V. A. Membrane curvature, lipid segregation, and structural transitions for phospholipids under dual-solvent stress. *Biochemistry* **1990**, *29*, 76–87.

(35) Kuzmin, P. I.; Zimmerberg, J.; Chizmadzhev, Y. A.; Cohen, F. S. A quantitative model for membrane fusion based on low-energy intermediates. *Proc. Natl. Acad. Sci. U.S.A.* **2001**, *98*, 7235–7240.

(36) Kozlovsky, Y.; Kozlov, M. M. Stalk model of membrane fusion: solution of energy crisis. *Biophys. J.* **2002**, *82*, 882–895.

(37) Markin, V. S.; Albanesi, J. P. Membrane fusion: stalk model revisited. *Biophys. J.* **2002**, *82*, 693–712.

(33) Hsieh, C. H.; Sue, S. C.; Lyu, P. C.; Wu, W. G. Membrane packing geometry of diphytanoylphosphatidylcholine is highly sensitive to hydration: phospholipid polymorphism induced by molecular rearrangement in the headgroup region. *Biophys. J.* **1997**, *73*, 870–877.

Finally, the very difficult phase problem in X-ray diffraction<sup>6</sup> can be solved by this method using neutron and D<sub>2</sub>O/H<sub>2</sub>O exchange. On the basis of the comparison of X-ray and neutron scattering amplitudes,<sup>24</sup> the high- and low-density regions for X-ray and neutron are congruent when hydrated with H<sub>2</sub>O. Therefore, one can often infer the X-ray phases from the neutron phases. One such example was shown by Turner et al.<sup>31</sup>

---

(38) The identification of any commercial product or trade name does not imply endorsement or recommendation by the National Institute of Standards and Technology.

**Acknowledgment.** We acknowledge the support of the National Institute of Standards and Technology, U.S. Department of Commerce, in providing the neutron research facilities used in this work. In particular, we thank Bryan Greenwald for his assistance at the NG7 SANS station during the experiment. This work was supported by NIH Grants GM55203 and RR14812 and by the Robert A. Welch Foundation (to H.W.H.). H.W.H. also thanks Misha Kozlov for discussion.

LA048720X